



HAL
open science

Comparison of the impact of fast charging on the cycle life of three lithium-ion cells under several parameters of charge protocol and temperatures

Romain Mathieu, Olivier Briat, Philippe Gyan, Jean-Michel Vinassa

► To cite this version:

Romain Mathieu, Olivier Briat, Philippe Gyan, Jean-Michel Vinassa. Comparison of the impact of fast charging on the cycle life of three lithium-ion cells under several parameters of charge protocol and temperatures. *Applied Energy*, 2021, 283, pp.116344. 10.1016/j.apenergy.2020.116344 . hal-04087500

HAL Id: hal-04087500

<https://hal.science/hal-04087500v1>

Submitted on 22 Jul 2024

HAL is a multi-disciplinary open access archive for the deposit and dissemination of scientific research documents, whether they are published or not. The documents may come from teaching and research institutions in France or abroad, or from public or private research centers.

L'archive ouverte pluridisciplinaire **HAL**, est destinée au dépôt et à la diffusion de documents scientifiques de niveau recherche, publiés ou non, émanant des établissements d'enseignement et de recherche français ou étrangers, des laboratoires publics ou privés.



Distributed under a Creative Commons Attribution - NonCommercial 4.0 International License

Comparison of the impact of fast charging on the cycle life of three lithium-ion cells under several parameters of charge protocol and temperatures

Romain Mathieu^{a,*}, Olivier Briat^a, Philippe Gyan^b, Jean-Michel Vinassa^a

^a Univ. Bordeaux, CNRS, Bordeaux INP, IMS, UMR 5218, F-33400, Talence, France

^b Renault, FR TCR LAB 012, Technocentre de Guyancourt, 1 avenue du golf, 78084, Guyancourt, France

* Corresponding author, telephone: +33540002613, email address: romain.mathieu@ims-bordeaux.fr

Abstract

Fast charging of lithium-ion batteries is crucial for electric vehicles. As the charge current is a known degradation factor, assessing the impact of fast charging on battery ageing under several operating conditions is necessary to derive usage strategies for system integrators. To bridge existing knowledge gaps, this article reports on a comparative experimental ageing study in fast charging conditions. Three cells, differing in their materials and energy densities, were investigated. The impacts of the following three parameters are compared on these cells: charge current, end-of-charge voltage, and ambient temperature. The results reveal that the impact of fast charging on cycle life strongly depends on battery materials and internal design. The degradation of two of the cells significantly increased when the charge current and voltage increased, whereas that of the third cell was nearly independent of these parameters. While considering thermal conditions, the ageing of each cell was minimised at a different temperature, either cold, moderate, or warm. An analysis of degradation root causes indicates that distinct dominant degradation mechanisms occurred depending on the cell materials. The cells with higher energy density had a lower cycle life (between 100 and 900 cycles) than the most high-power cell (more than 1700 cycles). Experimental results allow the identification of three strategies for reducing charging time while minimising battery degradation. These strategies present several contributions to the design of energy storage systems for electric vehicles, including the choice of a cell, design of thermal management systems, and design of optimised fast charging protocols.

Keywords: lithium-ion batteries; cycle life; fast charging; charge protocol; temperature sensitivity; energy density

1. Introduction

Fast charging of lithium-ion batteries is a crucial requirement for improving customer acceptance of battery electric vehicles (BEVs) and thus promote decarbonization of the transportation sector. After an important increase in battery pack energy, resulting in a greater driving range, intense efforts are now being devoted to achieve a higher charging power that will allow recovery of this driving range in a reduced time. To achieve this, a high-power charging infrastructure is currently deployed in several countries [1].

In addition to the infrastructure, fast charging capabilities are limited by several factors at the battery pack and cell levels [2]. Among them, battery ageing must be carefully considered. In the literature, high rates of charging current are known to accelerate several degradation mechanisms [3] such as lithium plating at the graphite negative electrode (NE) due to overpotentials [4], electrode particle fracture and structural degradation due to mechanical activity [5], or solid/electrolyte interphase (SEI) formation [6], fracture and reformation due to overpotentials, high temperatures and mechanical activity [7]. Thus, the repetition of fast charging events can have a substantial impact on the battery cycle life if not properly controlled.

In recent years, several important contributions were proposed to understand the impact of the charge on cycle life. It was mostly studied by accelerated ageing tests, taking as a parameter the charge current and in some cases the charge voltage, and using charge protocols such as constant current-constant voltage (CC-CV) or non-constant current profiles. Zhang studied the impact of several charging protocols on a high-energy cell and showed that degradation depends on the charge protocol in similar charging times [8]. However, the charging times of the tested protocols (of more than 150 minutes) are not representative of fast charging. Abdel Monem *et al.* found that several protocols have a lower degradation than the tested reference CC-CV protocol for a high-power cell [9]. Nonetheless, these protocols had a significantly longer charging time than the CC-CV reference, hence a lower average charge current which could explain the lower degradation.

In contrast, Ansean *et al.* determined that a significant increase in the charge current (and decrease in charge time) did not have a significant impact on the degradation of the studied high-power cell [10]. Mussa *et al.* reached a similar conclusion on another high-power cell [11]. They also observed that prolonging the charge at a high voltage with CV stage led to an increase of the degradation for this specific cell. The extensive study of Keil *et al.* showed that an increase in the charge current lead to an increase in degradation on three different high-power cells, although with different magnitudes [12]. They also studied the influence of the charge voltage and found that its increase lead to a more rapid degradation. Overall, the literature reports sometimes contradictory results but it can be concluded that charge current and charge voltage have varied impact on degradation depending on the cell. It is thus of significant value to compare several cell references in experimental studies.

According to our perspective, two important elements were ignored in the published literature in order to have a more complete understanding of the impact of fast charging on the cycle life of lithium-ion batteries: (i) the comparison of cells with different materials and/or energy/power orientations and (ii) the comparison at different ambient temperatures. While considering (i), electrode materials have different properties that impact their power or energy capabilities [13] and cells have different internal designs (such as electrochemical loading or electrode thickness) that impact their energy or power orientations [14]. Therefore, ageing mechanisms under high currents could depend on materials and internal design of each cell [15]. As most studies conducted experiments on a single cell reference, the results can hardly be transposed to other cells. Keil *et al.* reported ageing results from an extensive study that compared the impact of fast charging on the cycle life of three cells with different materials [12]. However, the tested cells were all oriented for high-power applications and had low energy densities, while high energy density is often preferred in BEVs for a high driving range. Thus, there is a requirement to study the impact of fast charging on high-energy cells. Another related question is whether high-energy cells are penalised for high charging currents when compared to high-power cells. Therefore, it is of interest to assess the sensitivity to fast charging for both energy and power cells in

comparable conditions to obtain insights on the appropriate choice of a cell for electric vehicle applications. While considering (ii), the vast majority of previous references on the impact of charging on cycle life achieved their ageing study at an ambient temperature of approximately 25 °C. However, degradation mechanisms strongly depend on the thermal conditions [16], and the charging of a vehicle is susceptible to occur at different temperatures depending on the regional weather and climate. Thus, there is a requirement for a better understanding of the fast charging impact on ageing over a wide range of temperatures in order to design optimized battery thermal management systems.

The objectives of this study are threefold. First, it analyses how different cells, which differ based on their materials and/or energy densities, are affected by fast charging. Then, it also investigates the impact of thermal conditions on the fast charging-induced degradation of these cells. The final objective is then to deduce strategies that can be exploited by battery system integrators to reduce electric vehicle charging time while avoiding detrimental battery degradation. To fulfil these objectives, this paper reports the results from an experimental ageing study by comparing the impact of CC-CV fast charging protocols on the degradation of three cells at different temperatures. The experimental study is presented in section 2. Degradation results in terms of capacity and resistance evolution are reported in section 3, and an analysis of the causes for the observed degradation follows in section 4. Finally, based on the obtained results, discussions on strategies for both faster charging and reduced degradation are presented in section 5.

2. Experimental ageing tests

This section describes the analysed cells and the achieved experimental ageing study with CC-CV fast charging protocols.

2.1 Studied cells

The comparative study was performed on three lithium-ion 18650 cells, referred to in this article as cells A, B, and C. These are commercial references, which are mass produced and obtained from recognised manufacturers. In hindsight, these considerations suggest a good repeatability of the results. The cells differ based on their materials and internal designs, which lead to different compromises between energy and power. Their characteristics are listed in **Table 1**.

Cell A is manufactured by LG with a nominal capacity of 3 Ah and nickel-rich $\text{LiNi}_{0.8}\text{Mn}_{0.1}\text{Co}_{0.1}\text{O}_2$ (NMC) as positive material and a graphite-silicon oxide blend (G-SiO) as negative material. It is a cell with significantly high energy, whose energy density (240 Wh kg^{-1}) is comparable with those of several different cells used in the battery packs of electric vehicles. Cell B is manufactured by SAMSUNG with a nominal capacity of 2.5 Ah and $\text{LiNi}_{0.8}\text{Co}_{0.15}\text{Al}_{0.05}\text{O}_2$ /graphite (NCA/G) electrode materials. Its energy density (200 Wh kg^{-1}) also shows that it is an energy cell. Cell C is manufactured by A123 SYSTEMS with a nominal capacity of 1.1 Ah and LiFePO_4 /graphite (LFP/G) electrode materials. It is designed for high-power applications, such as hybrid electric vehicles, and has a lower energy density (93 Wh kg^{-1}).

In commercial specifications, each manufacturer recommends a standard-charge current and fast-charge current. The fast-charge current is notably identical between the three cells with $I_{fc} = 4 \text{ A}$ (refer to **Table 1**). While considering the charging temperature range, manufacturers of cells A and B recommend not charging the cells at temperatures under $0 \text{ }^\circ\text{C}$, while the manufacturer of cell C recommends not charging the cell under $-30 \text{ }^\circ\text{C}$.

Table 1. Specifications of studied lithium-ion cells

Cell	A	B	C
Picture			
Reference	LG INR18650HG2	SAMSUNG INR1865025R	A123 APR18650M1B
Positive material	LiNi _{0.8} Mn _{0.1} Co _{0.1} O ₂ (NMC)	LiNi _{0.8} Co _{0.15} Al _{0.05} O ₂ (NCA)	LiFePO ₆ (LFP)
Negative material	Graphite + SiO (G-SiO)	Graphite (G)	Graphite (G)
Nominal capacity	3000 mAh	2500 mAh	1100 mAh
Resistance (AC 1 kHz)	15.0 mΩ	13.2 mΩ	12.0 mΩ
Energy density	240 Wh kg ⁻¹	200 Wh kg ⁻¹	93 Wh kg ⁻¹
Voltage range (U_{min} , U_{max})	2.5 to 4.2 V	2.5 to 4.2 V	2.0 to 3.6 V
Charge temperature range	0 to 50 °C	0 to 50 °C	-30 to 60 °C
Standard-charge current	1.5 A (C/2)	1.25 A (C/2)	1.5 A (1.36C)
Fast-charge current (I_{fc})	4 A (1.33C)	4 A (1.6C)	4 A (3.64C)

2.2 Initial characterisations

Apart from commercial specifications, possible additional characterisations of these cells can be performed with differential voltage (DV) analysis and electrochemical impedance spectroscopy (EIS). **Figure 1a** shows the DV curves obtained from a C/10 charge rate at 25 °C. Among the visible characteristics, the central peak of graphite is highlighted for each cell. This peak corresponds to a lithiation of 50 % of the graphite electrode [17] and signals the beginning of the last phase transition of graphite, where the potential is the closest to the

metallic lithium deposition reaction. It is located at approximately 57 % state-of-charge (SOC) for cells A and B, and approximately 72 % SOC for cell C, which indicates a difference in positive and negative electrode balancing between the cells. Owing to this excess of graphite, cell C is less sensitive to thermodynamic lithium plating compared to cells A and B, on their respective SOC scales. For kinetic plating (resistance driving the negative electrode below 0 V versus Li⁺/Li), negative electrode overvoltage during charge must be considered. **Figure 1b** shows the EIS spectra at 25 °C and 50 % SOC, which provides information on the internal resistance of the cells. The resistance values at 1 kHz (primarily due to conductivity phenomena) and at 1 Hz (primarily due to conductivity and interfacial electrochemical phenomena) vary with cells in the order of C < B < A, which is consistent with the energy densities of the cells. However, the resistance at 10 mHz (which adds the contribution of diffusion phenomena), is the highest for cell C, while it is similar for cells A and B. In general, cells with lower internal resistance can be charged faster [12], but more experimental data are required to determine if it provides any indication of ageing under fast charging conditions.

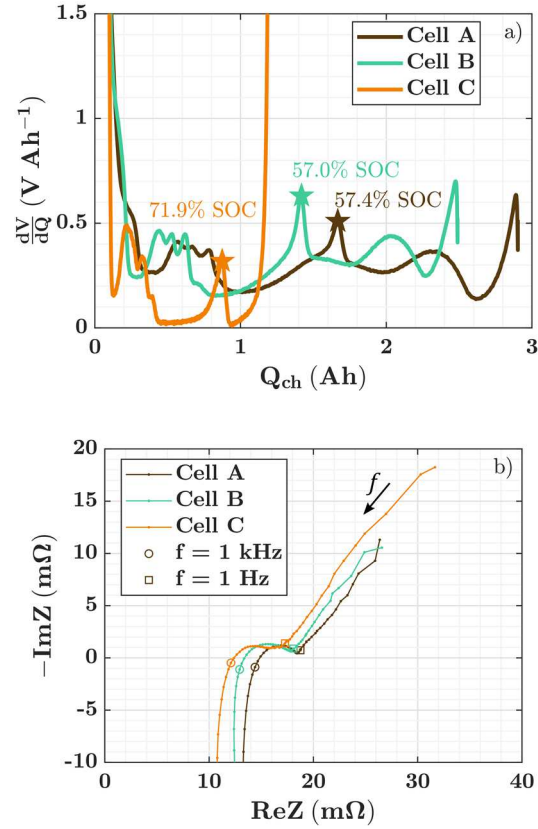


Figure 1. Information on cells at beginning of life: (a) differential voltage (DV) during a C/10 charge with the central graphite peak highlighted and (b) impedance spectra down to 10 mHz at 25 °C and 50% state-of-charge (SOC)

2.3 Charge protocols and test conditions

To identify the sensitivity of cells to fast charging, an ageing campaign was conducted according to the CC-CV charge protocol. This protocol is composed of two steps: first, a constant-current (CC) step until the voltage reaches U_{cv} , then a constant-voltage (CV) step during which the voltage is maintained at U_{cv} until the current drops to a value I_{cv} . The CC-CV protocol is often considered a reference protocol in the literature [12,18–20]. Its simplicity allows the measurement of fast charging degradation data under comparable conditions.

The current levels are defined in absolute ampere values, in contrast to being defined by C-rates, to avoid penalising the cells with higher capacity (form factor being identical here)

owing to the significantly higher electrode current density. This also ensures that tests are performed in a current range which is representative of fast charging for each cell. The end-of-charge current was also set at $I_{cv} = 300$ mA for each cell.

In order to obtain useful information on the possibilities of optimised fast-charge strategies, three key parameters were varied: the charge current I_{cc} , end-of-charge voltage U_{cv} and ambient temperature T_{amb} . The test conditions are listed in **Table 2** and discussed in the following paragraphs.

The charge current I_{cc} was varied according to three levels: 3, 4 and 5 A. These tests were performed at an ambient temperature of 25 °C. This allows the study of cell sensitivity to charge current around I_{fc} , while maintaining fast charging conditions. Then, the lowest tested C-rate is then 1C for cell A at 3 A, which is considered as a reference.

The end-of-charge voltage U_{cv} was varied according to two levels: U_{max} and $U_{max} - 100$ mV. The tests were predominantly performed at $U_{cv} = U_{max}$, which is considered as a complete charge, while one test was performed at $U_{cv} = U_{max} - 100$ mV at a charge current of 5 A and temperature of 25 °C. This last test was conducted to analyse the impact of a lower charge current on charging time, charged capacity, and degradation.

The ambient temperature T_{amb} was varied according to three levels: 5, 25, and 45 °C. These tests were performed at a charge current of 4 A. This allows the study of cell sensitivity to fast charging at temperatures that are representative of cold, mild, and hot climates, respectively, at an identical current value.

Table 2. Constant current-constant voltage (CC-CV) fast-charge ageing campaign: test conditions and charge data at beginning of life (averaged on the 10 first cycles)

Cell	Test conditions			Data at beginning of life	
	T_{amb} (°C)	I_{cc} (A)	U_{cv} (V)	t_{ch} (min)	SOC_f (%)
A	5	4 (1.33C)	4.2	66	91.4
	25	3 (1.00C)	4.2	70	98.0
	25	4 (1.33C)	4.2	61	96.2
	25	5 (1.67C)	4.2	52	95.7
	25	5 (1.67C)	4.1	46	83.3
	45	4 (1.33C)	4.2	53	97.8
B	5	4 (1.60C)	4.2	48	88.3
	25	3 (1.20C)	4.2	58	95.2
	25	4 (1.60C)	4.2	47	96.0
	25	5 (2.00C)	4.2	39	96.1
	25	5 (2.00C)	4.1	39	89.1
	45	4 (1.60C)	4.2	45	98.9
C	5	4 (3.64C)	3.6	24	89.3
	25	3 (2.73C)	3.6	27	95.6
	25	4 (3.64C)	3.6	21	98.2
	25	5 (4.55C)	3.6	17	97.4
	25	5 (4.55C)	3.5	20	99.7
	45	4 (3.64C)	3.6	20	94.8

In total, six test conditions were defined for each cell reference. As an example, **Figure 2** shows a comparison between the cell current, voltage, and charged capacity measured during the first charge at the conditions of 4 A and 25 °C. The total charge time t_{ch} and SOC at end-of-charge SOC_f for each cell and test condition are listed in **Table 2**.

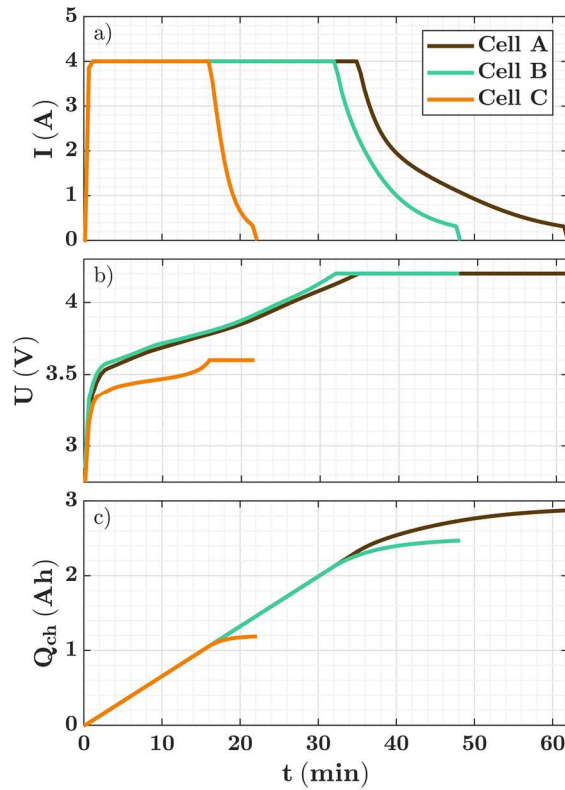


Figure 2. Comparison of current, voltage, and charged capacity as a function of time for tested cells, during first charge at $I_{cc} = 4 \text{ A}$ and $T_{amb} = 25 \text{ }^\circ\text{C}$

Generally, charging time is a function of the cell characteristics (capacity and internal resistance) and of the CC-CV protocol parameters (I_{cc} , U_{cv} , I_{cv}). Charging times t_{ch} vary between 17 and 70 min. It is significantly lower for cell C, primarily because of its lower capacity content (**Figure 2c**). Higher values of charge current I_{cc} reduce the charging time. For example, for cell A, when the charging current is 5 A instead of 3 A, the charging process is 18 min faster, at the same temperature. Higher values of temperature T_{amb} also help in reducing charging times, owing to faster kinetics and lower cell internal resistance [21]. For example, cell A is charged 13 min faster at 45 °C than at 5 °C at the same current level. The effect of lower U_{cv} on charging time depends on each cell reference. For cell A, t_{ch} is reduced, while it is unchanged for cell B and increased for cell C. This intriguing behaviour of t_{ch} at different charging voltages for cell C was also observed in [12] for another LFP/G cell and can be explained. In the CC stage, less time is logically required to

attain CV voltage when U_{cv} is lower. Thus, the CC stage has a lower charge time and, importantly, a lower amount of capacity charged. Hence, the CV stage has a longer charge time. This is due to the particular open-circuit potential of the LFP positive electrode, which is flat for the majority of the charge and then surges rapidly at the end of charge [22]. Owing to this surge at the end, the voltage window between 3.5 and 3.6 V represents nearly no capacity. This implies that to complete the CC-CV charge, nearly the totality of the capacity that is not charged during the CC stage has to be charged during the CV stage. Finally, it requires a longer time because during the CV stage, the current progressively decreases, achieving a lower mean current than the constant current I_{cc} . Moreover, the CV current is reduced even more because of the lower U_{cv} . Overall, the increase in the CV charge time than is more important than the decrease in the CC charge time, and the CC-CV charge time increases when U_{cv} is lower for this particular cell.

Generally, the end-of-charge SOC depends on the cell characteristics and end-of-charge parameters (U_{cv} , I_{cv}). Charging until the maximum voltage $U_{cv} = U_{max}$ at 25 and 45 °C results in a near-complete charge, i.e. between 95 and 98 % of the total capacity. Because of slower kinetics and higher cell resistance at the cold temperature (5 °C), the charge is partial, with SOC_f of approximately 90 %. Lowering the end-of-charge voltage U_{cv} results in a partial charge for cells A and B, but not for cell C, which results in an increased charge capacity. This particular behaviour on SOC_f at different charging voltages for cell C is also caused by the particular characteristic of the LFP open-circuit potential, as discussed above for t_{ch} .

2.4 Cycling procedure

Cycling tests were performed by repeating a charge-pause-discharge-pause sequence, where the charge step depended on previously described conditions, whereas the discharge and pauses protocols were identical for all tests and all cells. Discharges were performed according to a CC protocol with current $I_{dch} = 1.5$ A until the voltage reached U_{min} . This

discharge current is a compromise, chosen low to maximise the impact of charges on ageing when compared to that of discharges, but not too low to minimise the impact of calendar ageing when compared to that of cycle ageing. For cell A, it corresponds to a rate of $C/2$, indicating a discharge in approximately 2 h. Pause durations were set at 15 min after both charge and discharge steps. This value is a compromise between allowing thermal relaxation to T_{amb} before beginning charge or discharge and the minimisation of calendar degradation. Calendar degradation generally increases significantly at higher temperatures [23–28].

Two samples of each cell were used per cycling-test condition to provide an indication of repeatability. A simple sample was used at only the lower charge voltage condition (25 °C, 5 A, $U_{max} - 100$ mV). This test condition was incorporated after others, on which repeatability of degradation was verified and clear ageing trends could be identified. For this study, pristine cells were used and pre-screened. Preliminary inspections revealed that cell-to-cell variations in terms of capacity and internal resistance were low and could be neglected when compared to the difference in cycle life caused by different ageing conditions. Thus, clear conclusions could be drawn on the impact of different fast charging protocols on each cell reference.

With regard to the test equipment, cycling was performed using Biologic BCS-815 power benches connected electrically to the cells with Biologic BH-1i holders. Cells were placed inside Climats thermal chambers to regulate the temperature to the defined T_{amb} .

2.5 *Characterisation procedure*

Initial, periodic, and final characterisations were achieved at a temperature of 25 °C. Cycling tests were stopped around every 10 days for characterisations. Their goal was to provide a reference measure of capacity and resistance and their evolutions with ageing under comparable conditions.

Capacity Q_{dch} was measured during a CC discharge at C/10 until U_{min} , after the cells were charged by a CC charge at C/10 until U_{max} , and then allowed to rest for 30 min. Then, the cells were charged at 50 % SOC based on the measured capacity Q_{dch} and rested for 1 h. EIS experiments were finally performed for internal resistance measurements in galvanostatic mode with an excitation current of C/10 between frequencies of 10 kHz to 10 mHz.

2.6 End-of-test criterion

Because the studied cells have different capacities and an identical current is applied, cycles do not represent identical energies or durations. Therefore, the duration of the ageing tests is based, not on the number of cycles, but on the number of days, which was set to 180. For the cells that did not reach this duration, cycling was stopped after 50 % capacity loss. This choice allowed us to observe the influence of fast charging on the appearance of the final phase of ageing, characterised by a strong acceleration of degradation [29]. Resistance increase was not considered as a criterion to end the tests.

3. Analysis of ageing results

This section reports the impact of each controlled factor on the loss of capacity and increase in resistance, relative to their values at the initial characterisation. The capacity is measured in low current discharges of characterisations (Q_{dch}), as detailed in the previous section. The resistance is the real part of the impedance at 1 Hz ($Re\{Z_{1Hz}\}$, refer to the example in **Figure 1b**). The evolution of these degradation indicators is reported as a function of the number of cycles. They are not modified with the evolution of capacity; thus, a cycle represents an event of charge/discharge, as it is defined by its respective protocols and test conditions. Because of the lower capacity content of cell C, its cycle scale was reduced when compared to cells A and B, and 1000 cycles are indicated as a reference point

for comparison. Further, 30 % capacity loss is also indicated, which is used subsequently for life cycle analysis.

3.1 *Impact of charging current*

Figure 3 compares the influence of different charge currents, i.e. I_{cc} , on degradation. For each cell, different ageing trends and sensitivities to the charging current can be observed.

For cell A (**Figure 3a**), three stages of capacity loss can be distinguished: (1) high capacity loss at the beginning of life, (2) slower capacity loss at the middle of life, and (3) abrupt capacity loss acceleration leading to end-of-life. Losses during stage 1 are independent of I_{cc} . However, the charge current level impacts the ageing during stage 2 and the appearance of stage 3. The last stage appears much sooner when charging at 4 A (1.33C) when compared to 3 A (1C), for a 9 min gain in charging time (refer to **Table 2**). The capacity losses at 5 and 4 A are similar, indicating that currents superior to 3 A are particularly harmful for the cycle life of this cell. While considering the increase in resistance (**Figure 3d**), two stages of degradation can be distinguished: (1) slow resistance increase during stages 1 and 2 of capacity loss and (2) abrupt acceleration in resistance increase during stage 3 of capacity loss. The impact of the charge current on the resistance evolution is similar to that observed for capacity. In the following, this last stage of ageing, characterized by an abrupt acceleration of capacity loss and resistance increase which leads to end-of-life, is called a ‘failure’.

For cell B (**Figure 3b**), three stages of capacity loss can be distinguished as well; however, they correspond to different ageing trends when compared to those observed for cell A. The stage corresponding to the acceleration of capacity loss is the second stage for this cell. It is also less abrupt than that of cell A and is followed by a third stage where capacity loss slows significantly. The same three ageing stages can be observed for the resistance increase (**Figure 3e**). This suggests that cell B presents a softer failure when compared to cell A. Notably, it is observed on both ageing indicators that the charge current

I_{cc} has no influence on the degradation of cell B, despite a nearly 20 min difference in charging time between 3 A (1.2C) and 5 A (2C) (refer to **Table 2**), before the third and last stage. This last stage also happens when considerable degradation has already occurred, beyond the usual end-of-life criterion. Thus, the degradation of cell B is relatively independent of charge current and appears to be caused by cycling itself.

For cell C (**Figure 3c**), only two stages of capacity loss can be distinguished. These correspond to stages 2 and 3 of cell A. Thus, the second stage is similar to the failure stage observed for cell A, leading to end-of-life, and is observed at 4 A (3.64C) and 5 A (4.55C). Capacity loss is considerably accelerated from 4 to 5 A for a 4 min gain in charge time (refer to **Table 2**). While considering the increase of resistance (**Figure 3f**), two stages of degradation can be distinguished and a similar sensitivity to the charge current can be observed for capacity loss. During the first stage, this cell presented a significantly low increase in resistance when compared to the two other cells (lower than 15 %). A more significant increase in resistance increase is observed during the failure stage, as observed at 5 A.

For the three cells, the capacity loss and resistance increase followed similar trends at different charging currents. The same observation was made for the two other controlled ageing factors. Hence, only capacity loss is shown and considered in the rest of this section for the sake of conciseness.

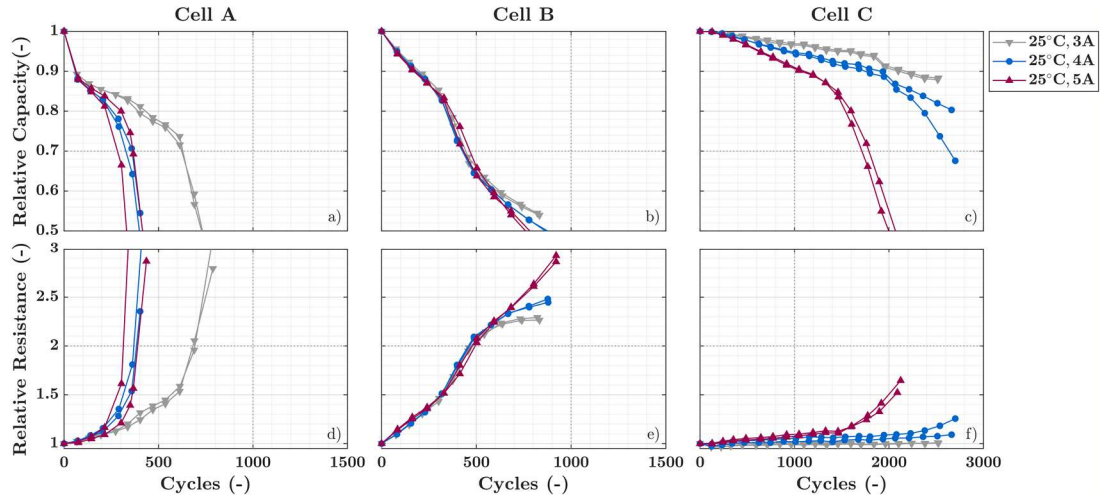


Figure 3. Impact of charge current I_{cc} on cycle life: relative capacity (top) and relative resistance (bottom) as a function of number of cycles at 25 °C and different values of I_{cc}

3.2 Impact of charging voltage

Figure 4 compares the influence of different end-of-charge voltages U_{cv} on degradation. Similar ageing trends and sensitivities to U_{cv} can be observed as described previously for different charge currents for each cell reference.

For cell A, a reduction in the charge voltage of 100 mV resulted in a partial charge, with approximately 83 % capacity being charged compared to the previous 96 %, and reduced duration of approximately 46 min when compared to 52 min (refer to **Table 2**). Within respect to degradation, the capacity loss is generally inferior when compared to the charge at U_{max} (**Figure 4a**). It is relatively close during the first two stages of ageing for the two conditions. However, the reduction of U_{cv} considerably delayed the appearance of the third stage and the failure. This result suggests that reducing the charging voltage value can be useful for this cell, as it allows both lower charge time and lower degradation with the drawback of a lower capacity charged.

For cell B, the reduction of U_{cv} also resulted in a partial charge, with approximately 89 % of charged capacity when compared to the previous 96 %; however, the durations of

approximately 39 min (refer to **Table 2**). For degradation, a trend similar to that observed at different charge currents can be observed, that is the level of U_{cv} had no influence on capacity loss apart from a significantly advanced ageing state (**Figure 4b**). Lowering the charging voltage is of less interest for this cell, as it resulted in less usable capacity for no significant reduction in charging time and degradation.

Conversely, for cell C, the reduction in U_{cv} resulted in a more complete charge, with approximately 100 % charged capacity when compared to the previous 97 %, and a longer duration of approximately 20 min when compared to 17 min (refer to **Table 2**). While considering the degradation, the capacity loss decreased significantly with a decrease in U_{cv} (**Figure 4c**). After 180 days of cycling, no failure was observed at 25 °C, 5 A, $U_{max} - 100$ mV. Interestingly, the capacity loss is significantly similar to that under the conditions of 25 °C, 3 A, U_{max} (refer to **Figure 3c**) for a reduction in charge time by 7 min. This comparison suggests that it is beneficial for this cell to perform charging at a higher current but at a lower end-of-charge voltage to reduce charging time significantly while also improving durability.

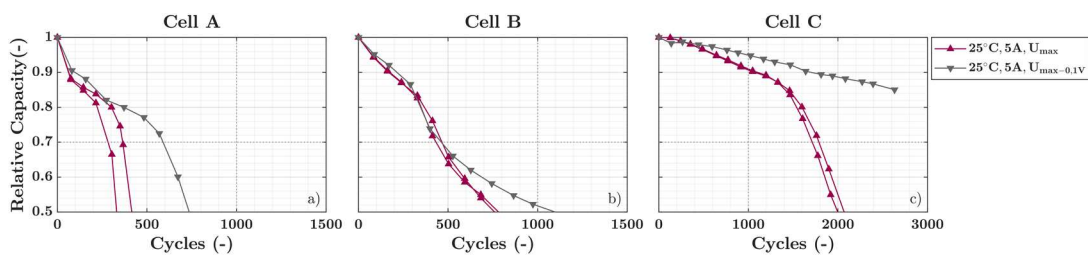


Figure 4. Impact of end-of-charge voltage U_{cv} on cycle life: relative capacity as a function of number of cycles at 25 °C, 5 A and different values of U_{cv}

3.3 Impact of ambient temperature

Figure 5 compares the impact of charging at different ambient temperatures T_{amb} for identical values of charge current ($I_{cc} = 4 \text{ A}$). Significant differences in ageing trends were observed.

For cell A (**Figure 5a**), the impact of thermal conditions on cycle ageing was strong. At the coldest studied temperature (5 °C), the cell was abruptly in a state of failure with a massive capacity loss from the beginning. Conversely, at the hottest temperature (45 °C), the capacity loss was significantly decreased and no failure was observed during the 180 days of cycling. At 45 °C, the relative capacity retention followed a trend similar to calendar ageing [30,31]. For this cell, fast charging at high temperatures (superior to 25 °C) was thus beneficial for both lower charge time (refer to **Table 2**) and degradation, whereas fast charging at low temperatures (less than 25 °C) resulted in a significantly rapid degradation.

For cell B (**Figure 5b**), the impact of charging at various temperatures was more complex than of cell A. The degradation was the highest at 45 °C at the beginning of life, but then became the most important at 25 °C, below approximately 80 % relative capacity. No stage of capacity loss acceleration was visible at 45 °C, similar to cell A. At 5 °C, a stage of capacity loss acceleration was observed at approximately 85 % of the relative capacity, but less significantly than at 25 °C. Notably, the degradation was the lowest at the coldest studied temperature. The degradation of this cell, which was relatively independent of charge current, was not significantly affected by fast charging at low temperatures.

For cell C (**Figure 5c**), the impact of fast charging at various temperatures demonstrated different trends than the two previous cells. At the beginning of cycling, the degradation was higher at the coldest temperature (5 °C). However, below approximately 85 % of the remaining capacity, degradation became more important at the highest temperature (45 °C). Contrary to cell A, a failure was observed at 45 °C for this cell, where it appeared first. The last stage of ageing for this cell also appeared at 5 °C, and then began at 25 °C, at which the

capacity loss was the lowest. Thus, it is then preferable to charge cell C at a moderate temperature, as degradation increased for both higher and lower temperatures.

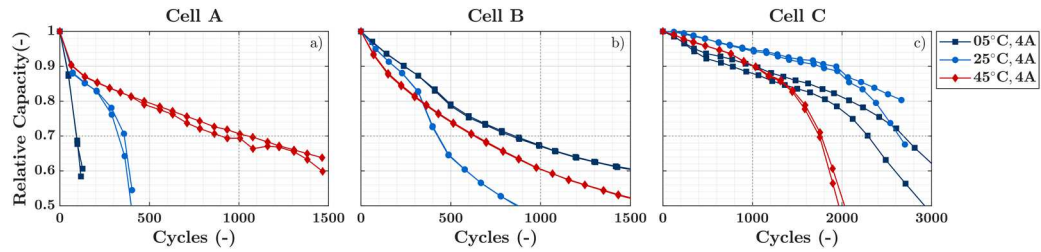


Figure 5. Impact of ambient temperature T_{amb} on cycle life: relative capacity as a function of number of cycles at 4 A and different values of T_{amb}

3.4 Cycle life analysis

A cycle life analysis was performed to highlight the impact of fast charging on durability and to understand which parameters are important to control during charging depending on the cell reference. Here, a comparison is proposed under an identical ageing criterion of 30 % capacity loss. The number of cycles to reach this criterion is illustrated in **Figure 6** for each cell and test condition.

The impacts of the charge current I_{cc} and end-of-charge voltage U_{cv} (top portion of **Figure 6**) are similar respective to each cell reference. The cycle life of cells A (NMC/G-SiO) and C (LFP/G) was highly influenced by the charge current and voltage level. For cell A, increasing I_{cc} from 3 A (1C) to 4 A (1.33C) nearly halved the cycle life (**Figure 6a**). Conversely, reducing U_{cv} from 4.2 to 4.1 V (with $I_{cc} = 4$ A, 1.67C) more than doubled it. This shows how strictly both the charge current and voltage have to be controlled in fast charging conditions in order to improve durability. In contrast to the other two cells, the cycle life of cell B (NCA/G) was nearly independent of both I_{cc} and U_{cv} in our study (**Figure 6b**). While considering the cycle life of each cell in general, the fast charging process damaged the cells with higher energy density (cells A and B) rather rapidly. Their

cycle life consisted of only a few hundred cycles, varying between 283 and 623 cycles for cell A and between 426 and 462 cycles for cell B. Conversely, the cycle life of cell C was superior with 1700 cycles for all conditions, while two conditions were far from achieving 30 % of capacity loss after 180 days of tests and more than 2500 cycles (**Figure 6c**, **3c** and **4c**). This suggests that cells oriented for high-power applications generally have a significantly longer cycle life under fast charging conditions, compared to cells oriented for energy applications.

The impact of fast charging at different ambient temperatures T_{amb} (bottom portion of **Figure 6**) demonstrates significantly contrasting results between the three cell references. The cycle life of cell A was the most highly dependent on thermal conditions (**Figure 6d**). It was indeed increased by nearly a factor of 10 between 5 and 45 °C, ranging from 92 to 899 cycles. The cycle lives of cells B and C were also dependent on the temperature, but to a lesser extent. For cell B, the number of cycles before reaching the criterion varied from 426 to 838 (**Figure 6e**), while it was between 1746 and 2636 for cell C (**Figure 6f**). At the three analysed levels of T_{amb} studied, it is notable that degradation under fast charging conditions was minimised at different temperatures: 45 °C for cell A, 5 °C for cell B, and 25 °C for cell C.

The next section presents an investigation of the observations formulated in this section regarding different ageing trends and sensitivities to controlled factors for the three cell references.

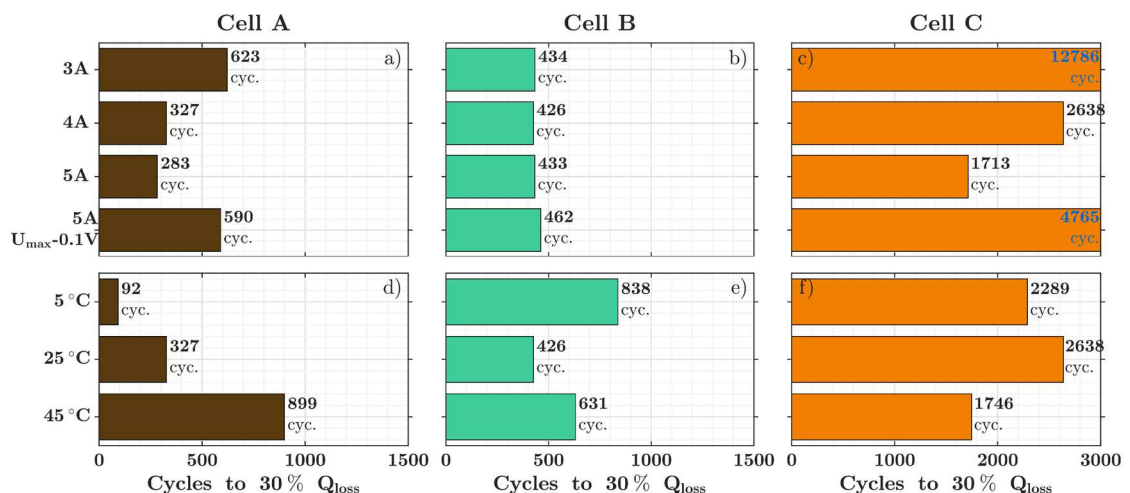


Figure 6. Cycle life analysis: number of cycles to reach 30 % of capacity loss at (top) different values of I_{cc} and U_{cv} ($T_{amb} = 25\text{ }^{\circ}\text{C}$) and at (bottom) different values T_{amb} ($I_{cc} = 4\text{ A}$ and $U_{cv} = U_{max}$). For each test condition, the reported number is the minimum of the two samples. For the two conditions that did not reach the criterion during cycling tests, an extrapolation of data was performed (number of cycles is represented in blue).

4. Analysis of degradation causes

This section presents an analysis of the causes of degradation based on information obtained during periodical characterisations at $25\text{ }^{\circ}\text{C}$ (refer to section 2.4) and non-intrusive analysis methods. The employed methods are DV, incremental capacity (IC), and EIS [17,32–38]. They provide useful information on the causes of capacity loss and resistance increase, which helps to identify ageing mechanisms. For DV and IC analyses, features were attributed to the positive (PE) or negative electrode (NE) and labelled as described in **Figure 7**.

For each cell, one example for one test condition was chosen, as illustrated in **Figure 7**, and explained subsequently to provide a representative perspective of the ageing modes of each cell. The DV, IC and EIS curves of all other conditions are provided as supplementary files for the interest of the reader (refer to **Appendix A**). Generally, the complete analysis suggests that degradation modes are the same between tests at different charge current/voltage values for a given cell, but with different magnitudes. However, they can differ between tests at different temperatures. Thus, one case at $25\text{ }^{\circ}\text{C}$ is compared for each cell reference in **Figure 7**, and the reader can view the eventual outliers at other temperatures in the supplementary figures. As shown in section 3, cell C degrades considerably less rapidly between periodical characterisations than cells A and B. Thus, we chose to compare the case with the highest charge current for cell C (5 A) with the case with the lowest charge current for cells A and B (3 A), in order to yield the most visual information on the degradation causes of each cell reference.

4.1 Cell A

Cell A comprises a nickel-rich NMC PE and a blended electrode-SiO NE [38]. The three previously described (refer to section 3.1) stages of ageing of cell A can be distinguished in these curves as well (left column of **Figure 7**). Between the first and second characterisations (first stage), degradation appears to primarily occur from the loss of lithium inventory (LLI). It is visible in the DV curves (**Figure 7a**), where all NE characteristics are shifted to the left in similar proportions, and in the IC curves (**Figure 7d**), where the peaks $P_{6_{NE}} \star P_{1_{PE}}$ and $P_{5_{NE}} \star P_{1_{PE}}$ are shifted towards higher voltages; moreover, the peak $P_{2_{NE}} \star P_{2_{PE}}$ loses amplitude and peak $P_{1_{NE}} \star P_{4_{PE}}$ stays constant [17]. These observations and the fact that the important capacity losses during this stage were independent of the current level (refer to **Figure 3a**) suggest capacity loss due to the initial formation of an SEI that was not complete at the beginning of life. During the second and third stages of ageing, the curves suggest a relationship between the LLI and the loss of active matter at the negative electrode (LAM_{NE}). During the second stage (between approximately 90 and 75 % of the remaining capacity), all previously described features of LLI continue at a slower rate when compared to the first stage, while the LAM_{NE} is visible in the IC curves (**Figure 7d**), where the peak $P_{1_{NE}} \star P_{4_{PE}}$ begins to lose amplitude [38]. During the third stage (below 75% remaining capacity), these phenomena strongly accelerate and NE features are no longer visible in the DV curves (**Figure 7a**). These observations suggest that the degradation primarily occur owing to the NE for this cell. The reason for the acceleration of capacity fading in the third stage could occur owing to the relationship between the LLI and the LAM_{NE} , as explained in [39]. Because of the excess graphite electrode at the beginning of life, the LAM_{NE} does not affect capacity fading during the second stage. However, when sufficient LAM_{NE} has occurred, it starts to limit the charge and the NE starts to become fully lithiated before 100 % SOC. Because the excess of the NE is consumed, the LAM_{NE} becomes visible and the capacity fade should follow the rate of this degradation mode. However, the NE shortage is compensated by the available lithium

inventory at the end of charge, inducing LLI. The free lithium ions then replace the missing capacity under two different modes: reversible and irreversible lithium plating. This irreversible part leads to increased LLI and the acceleration of capacity fade witnessed in the third stage. This could be an explanation of the failure mechanism for this cell. This is consistent with the fact that capacity loss is accelerated by higher charge currents (refer to **Figure 3a**) and lower temperatures (refer to **Figure 5a**). This is also consistent with the lower degradation observed when setting a lower charge voltage cut-off (**Figure 4a**). A lower voltage cut-off increases the amount of LAM_{NE} required for thermodynamic plating to start, and thus delays the accelerated stage.

While considering the EIS spectra (**Figure 7g**), during the two first stages of ageing, an increase in ohmic resistance can be observed (the spectrum is shifted to the right), which is consistent with the LLI and conductivity loss due to electrolyte degradation as well as a broadening of the semicircle of the mid-frequencies, which indicates the growth of passive films or electrochemical kinetics loss. During the last stage of degradation, a massive shift of the spectra to the right can be observed. This indicates a substantial conductivity loss, which could suggest an important degradation of the electrode structure, which is caused by mechanical degradation. Thus, massive mechanical degradation could thus also be a concurrent failure mechanism. The fact that no failure was observed at 45 °C (refer to **Figure 5a** and **S4**) could be explained by the fact that elevated temperatures expand the crystalline structure of the electrodes [40], which facilitates lithium insertion and reduces the amplitude of volume change and results in mechanical degradation as well as reduces the risk of lithium plating.

In summary, these results suggest that the degradation of cell A during fast charging is primarily due to the LLI and LAM_{NE} , which could be caused by irreversible lithium plating and mechanical degradation.

4.2 Cell B

Cell B comprises an NCA PE and a graphite NE [37]. The degradation of cell B is more progressive. The analysis hints that it occurs owing to a combination of the LLI and degradation of the PE. The LLI is particularly visible in the IC curves (**Figure 7e**), where the peak $P5_{NE} \star P1_{PE}$ shifts towards a higher voltage and then loses amplitude [41]. While considering the degradation of the PE, there appears to be a concurrent occurrence of two modes of degradation: loss of active matter at the PE (LAM_{PE}) and degradation of PE kinetics. The LAM_{PE} is visible at the beginning of cycling (between 100 and 85 % remaining capacity), first in the DV curves (**Figure 7b**), where NE peaks stay constant while all PE features are shifted to the left, and in the IC curves (**Figure 7e**), where the peaks $P2_{NE} \star P2_{PE}$, $P1_{NE} \star P3_{PE}$, and $P1_{NE} \star P4_{PE}$ lose amplitude [41]. Because of the capacity loss on the PE, the NE is decreasingly lithiated to a high SOC with ageing, as can be observed with the positions of peak $P1_{NE}$ and slope S_{PE} (**Figure 7b**). This can be an explanation for the low sensitivity of this cell degradation to charge currents/voltages and low temperatures, as thermodynamic lithium plating is decreasingly likely to occur with ageing. Moreover, it could also be the result of kinetic limitation from the PE. The degradation of the PE kinetics can especially be observed in the IC curves (**Figure 7e**), where all four marked peaks shifted towards higher voltages and the peaks $P2_{NE} \star P2_{PE}$, $P1_{NE} \star P3_{PE}$, and $P1_{NE} \star P4_{PE}$ are broadened [41]. This degradation of the PE kinetics is also consistent with the massive resistance increase observed for this cell.

In the EIS spectra (**Figure 7h**), it is possible to observe a progressive increase in ohmic resistance, which indicates conductivity loss, and, especially, the appearance and growth of a second semicircle at low frequencies, which indicates slower electrochemical or diffusion kinetics. When compared to the other two cells, the increase in resistance of cell B is significant. Given the information retrieved from the DV and IC curves, it can be inferred that this resistance increase primarily occurs owing to a phenomenon in the PE. Tsai *et al.* achieved precise measurements of the NMC and NCA particles and determined that NCA

particles were significantly more susceptible to fractures caused by mechanical activity [42], which could be a cause of the LAM_{PE} and kinetic limitations at the PE of cell B. These observations can also provide a second explanation for the low sensitivity of cell B degradation to charge currents/voltages and low temperatures: an important cell resistance, occurring primarily owing to the PE, results in reaching the voltage U_{cv} at a relatively low SOC, and thus achieving an early reduction of current due to the CV phase. As overpotentials are lower at the NE, this can effectively protect the graphite from kinetic lithium plating.

In summary, these results suggest that the degradation of cell B during fast charging and cycling is caused by LLI, LAM_{PE} , and slower PE kinetics, thereby primarily degrading the positive NCA electrode. This degradation of the PE can explain the ageing trends of this cell during fast charging observed in the previous section.

4.3 Cell C

Cell C comprises an LFP PE and a graphite NE [17]. The two stages of cell C degradation, which were previously discussed (refer to section 3.1), can also be observed in the DV and IC curves. The analysis indicates that the modes of degradation occur concurrently throughout ageing, but are significantly accelerated during the observed failure of the cell. The degradation modes appear to be the LLI and LAM_{NE} . These two effects were combined and are visible on the DV curves (**Figure 7c**), where all graphite characteristics are shifted to the left, and on the IC curves (**Figure 7f**), where all peaks demonstrate a reduction in amplitude. The PE is inconsequential on the IC curves owing to the flat potential curve of the LFP. As cell C degradation is sensitive to charge current and voltage (refer to **Figure 6**), it can be inferred that the LLI and LAM_{NE} relationship follows a similar pattern as that previously explained for cell A and in [39], causing irreversible lithium plating and the failure of the cell. A new peak appears below 70 % remaining capacity on DV (**Figure 7c**), which indicates that a new reaction begins to occur in the working voltage

window of this cell. Considering the important shift of the peak $P1_{NE}$ (which corresponds to a complete LiC_{12} phase) to the left, this reaction could be the complete lithiation of graphite (LiC_6). This could be the result of the LAM_{NE} and could ultimately increase the risk of thermodynamic lithium plating at low states-of-health. Notably, this effect is particularly visible for this cell under the test conditions at 5 °C (refer to **Figure S1** and **S3**).

In the EIS spectra (**Figure 7i**), an increase in the ohmic resistance can be observed. For cell A, a bigger and sudden increase in ohmic resistance occurs during the failure which could also be the result of structural degradation caused by mechanical activity. Nevertheless, this increase is less important for cell C, and generally, the resistance of this cell is considerably stable when compared to the other two cells.

In summary, these results suggest that the degradation of cell C during fast charging is primarily due to LLI and LAM_{NE} , and possibly caused by lithium plating and mechanical degradation.

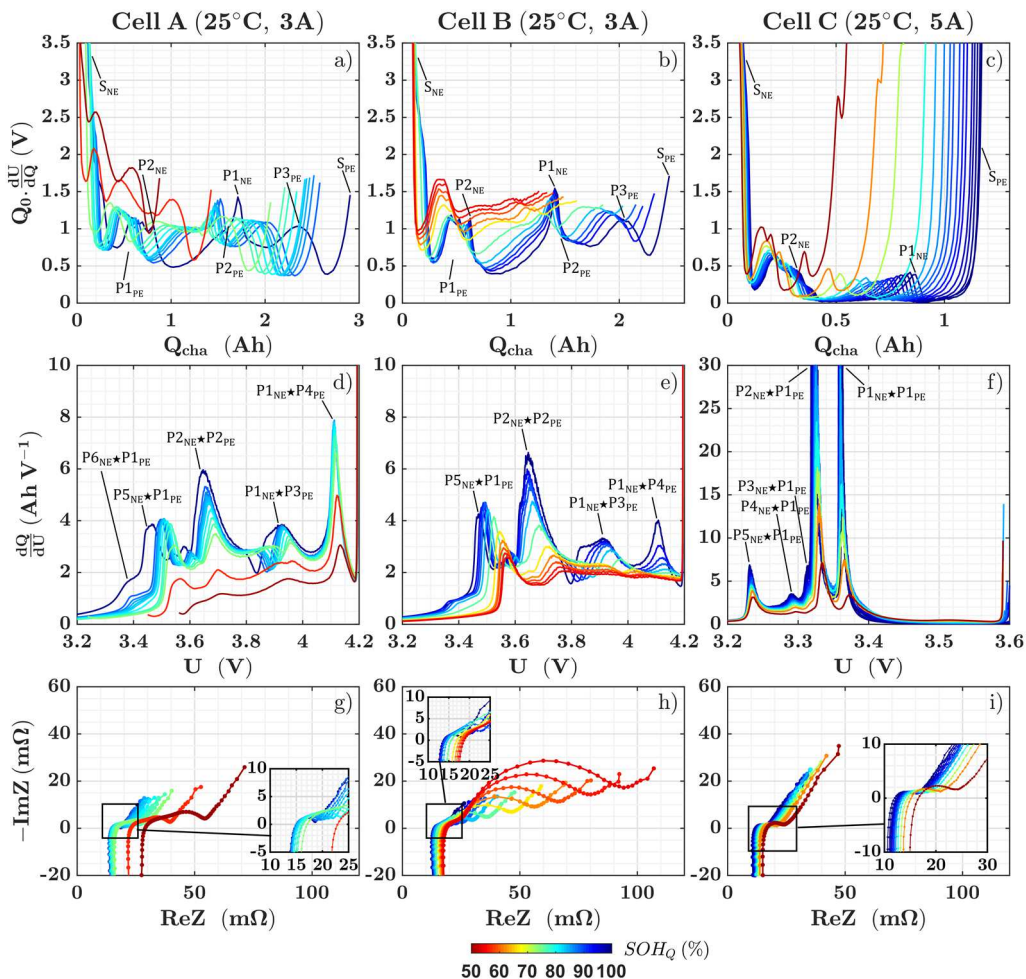


Figure 7. Analysis of degradation causes: (top) DV as a function of charged capacity, (middle) incremental capacity (IC) as a function of voltage and (bottom) impedance spectra as Nyquist plots, at different states-of-health (SOH_Q) for one test condition for each cell reference. For DV and IC curves, the characteristics of each electrode are indicated at the beginning of life (heavy blue line) and labelled as peaks (P) or slopes (S) of the positive (PE) or negative electrode (NE). The reader is advised that peaks in DV correspond to valleys in IC and vice versa; therefore, their labelling is independent and do not correspond to the same features. Peaks in DV correspond to a potential jump between two potential plateaus and are an addition of the two electrodes, whereas peaks in IC correspond to potential plateaus which indicate a transition between two different phases of the active material and are convolutions of the two electrodes (marked with ★).

5. Discussions on strategies for fast charging considering degradation management

The results of our comparative experimental study show that fast charging can have a significant impact on cycle life. However, three strategies for both charging time reduction and degradation mitigation can be identified for use in electric vehicles. These strategies include the choice of an appropriate cell reference, thermal management, and charging protocol.

5.1 Cell selection strategy

For electric vehicle applications, the choice of a cell for a battery pack is guided by multiple constraints such as raw materials, suppliers, cost, available energy, and, more recently, its ability to charge quickly. The primary parameters to be considered for a given cell are the employed materials and its internal design, which impacts its power and energy densities.

While considering the employed materials, the results indicate that the degradation of certain cells such as cell A (NMC/G-SiO) and cell C (LFP/G) is dependent on parameters that can be controlled, such as the charge current and voltage (refer to **Figure 6**). Thus, the charging protocol parameters can be optimised for charging in a reduced duration and to mitigate the impact of fast charging on degradation. Conversely, the degradation of certain cells such as cell B (NCA/G) is independent of these parameters, implying that there is limited room for the optimisation of the fast charging protocol.

While considering the internal design, one question that can be raised when comparing different cells is the benefit of using a cell reference with less energy density but with higher power density to achieve both significantly faster charging and maintaining a long lifetime. The results show that the cycle life of the high-power cell (cell C) is significantly less impacted by fast charging (refer to **Figure 6**) when compared to the cells with higher energy densities (cells A and B). However, this difference in cycle life is exacerbated by the conventional comparison in terms of number of cycles, because cycles for cell C represent a significantly lower usable energy, implying that more charges would be required to drive the same distance as using cell A or B. To highlight this, capacity losses were compared on a scale of cumulated discharged energy for one test condition of each cell, as illustrated in **Figure 8**. To contribute to the question raised, this comparison was performed between the lowest studied current for the cell with the highest energy density (cell A) and the highest studied current for the two other cells (cells B and C). This comparison shows that at a 67 % higher charge current (5 A versus 3 A), cell C attained 30 % capacity loss at a point similar to that of cell A, after approximately 5500 Wh were discharged. While considering the important increase in ageing for an increase from 4 to 5 A for cell C (refer to **Figure 3c**), the current of 5 A appears to be close to a limit for the fast charging of cell C. Thus, the comparison places the significantly higher cycle life of cell C into perspective, as the gain in charge current (67 %) for the same durability might not justify the loss of energy and autonomy (61 %, refer to **Table 1**) for vehicle users. Cell B at 5 A achieves 30 % capacity loss at a lower discharged energy of approximately 3500 Wh. The interest of this cell for

fast charging in electric vehicles is also diminished by its significant increase in resistance (refer to **Figure 3e** and **7h**), which progressively prolongs the charging time and increases heating inside the battery pack.

In conclusion, several aspects must be considered when selecting a cell for fast charging in an electric vehicle. The subsequent two strategies can also be considered for optimising the cycle life under fast charging, on a cell by cell basis.

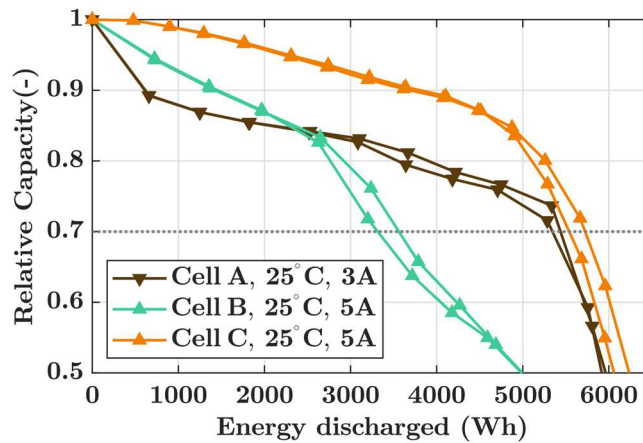


Figure 8. Comparison of relative capacity as a function to cumulated discharged energy for cell A (25 °C, 3 A) and cells B and C (25 °C, 5 A).

5.2 Thermal conditioning strategy

Generally, elevated temperatures decrease the internal resistance and thus promote reduced charging durations and charged capacities (refer to **Table 2**). The results of our experimental ageing study also show that at a given current rate, degradation can strongly depend on thermal conditions (refer to **Figure 6**). Thus, a conceivable strategy is to apply thermal management to determine the best compromise between performance and degradation in fast charging conditions.

The degradation of the cell with the highest energy density (cell A) was reduced at 45 °C, while that of the cell with the highest power density (cell C) was reduced at 25 °C. A possible explanation of this experimental finding can be obtained in a theoretical study by Yang *et al.* [43]. Based on an electrochemical model framework, the authors added an ageing model representing degradation as a competition between lithium plating (accelerated by low temperatures) and SEI growth (accelerated by high temperatures) to study the interdependence of energy density, charge rate, and temperature. By simulation, they determined that at a given charge current, there exists a temperature that minimises ageing; moreover, this temperature increases when the current rate and energy density (loading of active material) increase, which is consistent with our experimental observations. Other than SEI growth and lithium plating, additional ageing mechanisms worth considering in this case are the fracture of active materials or electrode structure degradation due to mechanical activity. Logically, as the host crystalline structure expands with increased temperature [40], lithium is more easily inserted, which reduces mechanical activity and subsequent damage. Thus, increasing the temperature can be considered as a way to sufficiently improve the kinetics of cell internal phenomena to withstand compatible charging rates. Another recent study by Yang *et al.* [44] confirmed experimentally that an NMC-LFP/G cell with an energy density of 209 Wh kg⁻¹ can withstand significantly high charge rates when using an elevated temperature during charge and reduced temperature during discharge, thereby minimising calendar degradation and SEI growth.

Thus, thermal management is a valuable strategy for the reduction of charging times. It consists of conditioning the cell in a temperature range that both promotes high electrochemical performance and low degradation. For NMC/G high-energy cell, this compromise would be effective at elevated temperatures (> 40 °C). This would sometimes require the heating of the battery pack, and the conditioning could be applied before, during and after the charge for the best results.

5.3 Optimised charging protocol strategy

The results show that the degradation of certain cells such as cells A and C highly depends on the charging protocol parameters (refer to **Figure 6**). Hence, optimising the charging protocol is another strategy to be considered for faster charging.

When the charge current increases, the charging time is reduced (refer to **Table 2**). However, because of kinetic limitations, the gains in charge duration would be reduced after a given level of current as the upper voltage limit would be reached and a transition to the CV stage occurs, which lowers the current. When the end-of-charge voltage increases, the charged capacity generally increases (refer to **Table 2**). Conversely, the degradation of cells such as cells A and C is accelerated when both the charge current and voltage increase (refer to **Table 2**). Therefore, the charging protocol parameters should be optimised to determine the best compromise between low charging time, high charged capacity/energy, and low degradation. As cells A and C are presumably sensitive to lithium plating (refer to section 4), charging protocols that allow adaptation of the charge current depending on the SOC during the charge could provide sensible improvements. This protocol would decrease the current decrease towards higher SOC, at a level compatible with a charging time constraint. Another possibility is to stop the charge at a lower SOC or lower end-of-charge voltage, at a level compatible with an energy constraint. On the other hand, it could be advantageous to adapt the charging protocol parameters when the state-of-health has significantly changed. It would help to avoid a failure of the cell, as observed in cell A (refer to section 3) and to further prolong durability.

Optimising the charging protocol is another important strategy. It finally brings together the three strategies identified here, as the charging protocol parameters should be first adapted to each cell reference characteristics and to the thermal conditions. It then consists of choosing the parameters that provide the best compromise between user requirements (low charging time and high recovered energy) and low degradation.

6. Conclusion

This article reports the results of an experimental ageing campaign of batteries in fast charging conditions in order to fill existing knowledge gaps. One novelty comes from the comparison of three commercial 18650 lithium-ion cells, which represent different electrode materials and different internal designs for cells oriented more towards energy or more towards power applications. The ageing campaign consisted of alternating a high current constant current-constant voltage charge and a lower current discharge. To identify the most important parameters to control during fast charging, three parameters were varied. On top of the charge current and the end-of-charge voltage, the ambient temperature was also studied to fill another gap in the current understanding. The results revealed that the impact of fast charging on cycle life depends considerably materials and design of each cell.

For each given cell, the impacts of the charge current and voltage were similar. For cells A ($\text{LiNi}_{0.8}\text{Mn}_{0.1}\text{Co}_{0.1}\text{O}_2/\text{graphite-SiO}$) and C ($\text{LiFePO}_4/\text{graphite}$), the increase in these two parameters decreased their cycle life, whereas the cycle life of cell B ($\text{LiNi}_{0.8}\text{Co}_{0.15}\text{Al}_{0.05}/\text{graphite}$) was nearly independent of these parameters. For example, for cell A, increasing the charge current by just 1 A (or 0.33C), halved the cycle life. For this cell, the end-of-charge voltage is an equally important parameter to be controlled for improving its durability. The causes of degradation were analysed by means of differential voltage, incremental capacity and electrochemical impedance spectroscopy analyses. These analyses indicated a negative electrode degradation for cells A and C, presumably caused by lithium plating and mechanical degradation, and a positive electrode degradation for cell B. This positive electrode degradation could have resulted in reduced lithiation of the negative electrode and a massive increase in impedance on the positive side, which can explain the low sensitivity of the ageing of this cell to charge current and voltage owing to a reduced risk of lithium plating.

The impacts of fast charging at different temperatures were more diverse. The cycle life of cell A was the most sensitive to thermal conditions, as cycle life was multiplied by a

factor of 10 at the same charge current when the temperature ranged from 5 to 45 °C. In particular, it was observed that the ageing of each cell was minimised at a different temperature among those studied: 45 °C for cell A, 5 °C for cell B, and 25 °C for cell C. For cell B, its low sensitivity to fast charging at the lower temperature can also be explained by the specific degradation of this cell and its low sensitivity to lithium plating. For cells A and C, this could be explained by a competition between ageing mechanisms accelerated by low temperatures (lithium plating, mechanical degradation) and high temperatures (growth of solid electrolyte interphase) that interplay with energy density. Cells with higher energy densities would thus require higher temperatures to withstand a given charging rate. In general, the results showed that fast charging has a strong impact on the cycle life of these cells. Cells with higher energy densities (cells A and B) were more affected as their cycle life varied between 100 and 900 cycles, while that of cell C was superior to 1700 cycles for all conditions. The durability advantage of the high-power cell is less important when comparing the degradation as a function of the accumulated discharge energy; however, it is still present.

For a practical electric vehicle application, the results and their analysis allowed the identification of three strategies for the reduction of charging time while minimising its impact on cycle life. These strategies include the choice of a cell reference, thermal conditioning during charge, and the optimisation of the charging protocol. These three strategies should be further optimised and finally coupled into the energy storage system to provide electric vehicle users with fast charging times and long battery lifetimes. This will make electric vehicles more attractive and contribute to the decarbonization of transportation.

Acknowledgements

This work received funding from the French National Association for Technological Research (ANRT) under grant CIFRE N° 2016/1200. The funding source had no involvement in any aspect of the study or report.

References

- [1] Till Bunsen, P. Cazzola, L. D'Amore, M. Gerner, S. Scheffer, R. Schuitmaker, et al., Global EV Outlook 2019 to electric mobility, 2019. www.iea.org/publications/reports/globalevoutlook2019/.
- [2] S. Ahmed, I. Bloom, A.N. Jansen, T. Tanim, E.J. Dufek, A. Pesaran, et al., Enabling fast charging – A battery technology gap assessment, *J. Power Sources*. 367 (2017) 250–262. <https://doi.org/10.1016/j.jpowsour.2017.06.055>.
- [3] N. Omar, M.A. Monem, Y. Firouz, J. Salminen, J. Smekens, O. Hegazy, et al., Lithium iron phosphate based battery - Assessment of the aging parameters and development of cycle life model, *Appl. Energy*. 113 (2014) 1575–1585. <https://doi.org/10.1016/j.apenergy.2013.09.003>.
- [4] Z. Li, J. Huang, B. Yann Liaw, V. Metzler, J. Zhang, A review of lithium deposition in lithium-ion and lithium metal secondary batteries, *J. Power Sources*. 254 (2014) 168–182. <https://doi.org/10.1016/j.jpowsour.2013.12.099>.
- [5] N. Lin, Z. Jia, Z. Wang, H. Zhao, G. Ai, X. Song, et al., Understanding the crack formation of graphite particles in cycled commercial lithium-ion batteries by focused ion beam - scanning electron microscopy, *J. Power Sources*. 365 (2017) 235–239. <https://doi.org/10.1016/j.jpowsour.2017.08.045>.
- [6] M.B. Pinson, M.Z. Bazant, Theory of SEI Formation in Rechargeable Batteries: Capacity Fade, Accelerated Aging and Lifetime Prediction, *J. Electrochem. Soc.* 160 (2013) A243–A250. <https://doi.org/10.1149/2.044302jes>.
- [7] I. Laresgoiti, S. Käbitz, M. Ecker, D.U. Sauer, Modeling mechanical degradation in lithium ion batteries during cycling: Solid electrolyte interphase fracture, *J. Power Sources*. 300

- (2015) 112–122. <https://doi.org/10.1016/j.jpowsour.2015.09.033>.
- [8] S.S. Zhang, The effect of the charging protocol on the cycle life of a Li-ion battery, *J. Power Sources*. 161 (2006) 1385–1391. <https://doi.org/10.1016/j.jpowsour.2006.06.040>.
- [9] M. Abdel Monem, K. Trad, N. Omar, O. Hegazy, B. Mantels, G. Mulder, et al., Lithium-ion batteries: Evaluation study of different charging methodologies based on aging process, *Appl. Energy*. 152 (2015) 143–155. <https://doi.org/10.1016/j.apenergy.2015.02.064>.
- [10] D. Ansean, M. Dubarry, A. Devie, B.Y. Liaw, V.M. Garcia, J.C. Viera, et al., Fast charging technique for high power LiFePO₄ batteries: A mechanistic analysis of aging, *J. Power Sources*. 321 (2016) 201–209. <https://doi.org/10.1016/j.jpowsour.2016.04.140>.
- [11] A.S. Mussa, M. Klett, M. Behm, G. Lindbergh, R.W. Lindström, Fast-charging to a partial state of charge in lithium-ion batteries: A comparative ageing study, *J. Energy Storage*. 13 (2017) 325–333. <https://doi.org/10.1016/j.est.2017.07.004>.
- [12] P. Keil, A. Jossen, Charging protocols for lithium-ion batteries and their impact on cycle life—An experimental study with different 18650 high-power cells, *J. Energy Storage*. 6 (2016) 125–141. <https://doi.org/10.1016/j.est.2016.02.005>.
- [13] N. Nitta, F. Wu, J.T. Lee, G. Yushin, Li-ion battery materials: Present and future, *Mater. Today*. 18 (2015) 252–264. <https://doi.org/10.1016/j.mattod.2014.10.040>.
- [14] M.J. Lain, J. Brandon, E. Kendrick, Design strategies for high power vs. High energy lithium ion cells, *Batteries*. 5 (2019). <https://doi.org/10.3390/batteries5040064>.
- [15] M.R. Palacín, Understanding ageing in Li-ion batteries: A chemical issue, *Chem. Soc. Rev.* 47 (2018) 4924–4933. <https://doi.org/10.1039/c7cs00889a>.
- [16] T. Waldmann, M. Wilka, M. Kasper, M. Fleischhammer, M. Wohlfahrt-Mehrens, Temperature dependent ageing mechanisms in Lithium-ion batteries - A Post-Mortem study, *J. Power Sources*. 262 (2014) 129–135. <https://doi.org/10.1016/j.jpowsour.2014.03.112>.
- [17] M. Dubarry, C. Truchot, B.Y. Liaw, Synthesize battery degradation modes via a diagnostic and prognostic model, *J. Power Sources*. 219 (2012) 204–216. <https://doi.org/10.1016/j.jpowsour.2012.07.016>.
- [18] T. Waldmann, M. Kasper, M. Wohlfahrt-Mehrens, Optimization of Charging Strategy by Prevention of Lithium Deposition on Anodes in high-energy Lithium-ion Batteries - Electrochemical Experiments, *Electrochim. Acta*. 178 (2015) 525–532.

<https://doi.org/10.1016/j.electacta.2015.08.056>.

- [19] M. Abdel-Monem, K. Trad, N. Omar, O. Hegazy, P. Van den Bossche, J. Van Mierlo, Influence analysis of static and dynamic fast-charging current profiles on ageing performance of commercial lithium-ion batteries, *Energy*. 120 (2017) 179–191. <https://doi.org/10.1016/j.energy.2016.12.110>.
- [20] X. Fleury, M.H. Noh, S. Geniès, P.X. Thivel, C. Lefrou, Y. Bultel, Fast-charging of Lithium Iron Phosphate battery with ohmic-drop compensation method: Ageing study, *J. Energy Storage*. 16 (2018) 21–36. <https://doi.org/10.1016/j.est.2017.12.015>.
- [21] W. Waag, S. Käbitz, D.U. Sauer, Experimental investigation of the lithium-ion battery impedance characteristic at various conditions and aging states and its influence on the application, *Appl. Energy*. 102 (2013) 885–897. <https://doi.org/10.1016/j.apenergy.2012.09.030>.
- [22] A. Eddahech, O. Briat, J.M. Vinassa, Performance comparison of four lithium-ion battery technologies under calendar aging, *Energy*. 84 (2015) 542–550. <https://doi.org/10.1016/j.energy.2015.03.019>.
- [23] I. Baghdadi, O. Briat, J.Y. Delétage, P. Gyan, J.M. Vinassa, Lithium battery aging model based on Dakin's degradation approach, *J. Power Sources*. 325 (2016) 273–285. <https://doi.org/10.1016/j.jpowsour.2016.06.036>.
- [24] P. Keil, S.F. Schuster, J. Travi, A. Hauser, R.C. Karl, A. Jossen, Calendar Aging of Lithium-Ion Batteries I . Impact of the Graphite Anode on Capacity Fade, *J. Electrochem. Soc.* 163 (2016) 1872–1880. <https://doi.org/10.1149/2.0411609jes>.
- [25] E. Redondo-Iglesias, P. Venet, S. Pelissier, Eyring acceleration model for predicting calendar ageing of lithium-ion batteries, *J. Energy Storage*. 13 (2017) 176–183. <https://doi.org/10.1016/j.est.2017.06.009>.
- [26] M. Dubarry, N. Qin, P. Brooker, Calendar aging of commercial Li-ion cells of different chemistries – A review, *Curr. Opin. Electrochem.* 9 (2018) 106–113. <https://doi.org/10.1016/j.coelec.2018.05.023>.
- [27] C. Lin, J. Cabrera, F. Yang, M. Ling, K. Tsui, D. Science, et al., Battery state of health modeling and remaining useful life prediction through time series model, 275 (2020).
- [28] P.P. Mishra, A. Latif, M. Emmanuel, Y. Shi, K. McKenna, K. Smith, et al., Analysis of

- degradation in residential battery energy storage systems for rate-based use-cases, *Appl. Energy*. 264 (2020). <https://doi.org/10.1016/j.apenergy.2020.114632>.
- [29] S.F. Schuster, T. Bach, E. Fleder, J. Müller, M. Brand, G. Sextl, et al., Nonlinear aging characteristics of lithium-ion cells under different operational conditions, *J. Energy Storage*. 1 (2015) 44–53. <https://doi.org/10.1016/j.est.2015.05.003>.
- [30] R. Mathieu, I. Baghdadi, O. Briat, P. Gyan, J.-M. Vinassa, D-optimal design of experiments applied to lithium battery for ageing model calibration, *Energy*. 141 (2017) 2108–2119. <https://doi.org/10.1016/j.energy.2017.11.130>.
- [31] I. Mathews, B. Xu, W. He, V. Barreto, T. Buonassisi, I.M. Peters, Technoeconomic model of second-life batteries for utility-scale solar considering calendar and cycle aging, *Appl. Energy*. 269 (2020). <https://doi.org/10.1016/j.apenergy.2020.115127>.
- [32] C.R. Birkl, M.R. Roberts, E. McTurk, P.G. Bruce, D.A. Howey, Degradation diagnostics for lithium ion cells, *J. Power Sources*. 341 (2017) 373–386. <https://doi.org/10.1016/j.jpowsour.2016.12.011>.
- [33] P. Keil, *Aging of Lithium-Ion Batteries in Electric Vehicles*, Technische Universität München, 2017. <https://doi.org/10.1029/2010GM000932>.
- [34] C. Pastor-Fernández, K. Uddin, G.H. Chouchelamane, W.D. Widanage, J. Marco, A Comparison between Electrochemical Impedance Spectroscopy and Incremental Capacity-Differential Voltage as Li-ion Diagnostic Techniques to Identify and Quantify the Effects of Degradation Modes within Battery Management Systems, *J. Power Sources*. 360 (2017) 301–318. <https://doi.org/10.1016/j.jpowsour.2017.03.042>.
- [35] C. Weng, X. Feng, J. Sun, H. Peng, State-of-health monitoring of lithium-ion battery modules and packs via incremental capacity peak tracking, *Appl. Energy*. 180 (2016) 360–368. <https://doi.org/10.1016/j.apenergy.2016.07.126>.
- [36] B. Jiang, H. Dai, X. Wei, Incremental capacity analysis based adaptive capacity estimation for lithium-ion battery considering charging condition, *Appl. Energy*. 269 (2020). <https://doi.org/10.1016/j.apenergy.2020.115074>.
- [37] A. Devie, M. Dubarry, Durability and reliability of electric vehicle batteries under electric utility grid operations. Part 1: Cell-to-cell variations and preliminary testing, *Batteries*. 2 (2016) 1–13. <https://doi.org/10.3390/batteries2030028>.

- [38] D. Anseán, G. Baure, M. González, I. Cameán, A.B. García, M. Dubarry, Mechanistic investigation of silicon-graphite/LiNi_{0.8}Mn_{0.1}Co_{0.1}O₂ commercial cells for non-intrusive diagnosis and prognosis, *J. Power Sources*. 459 (2020). <https://doi.org/10.1016/j.jpowsour.2020.227882>.
- [39] M. Dubarry, G. Baure, D. Anseán, Perspective on State-of-Health Determination in Lithium-Ion Batteries, *J. Electrochem. Energy Convers. Storage*. 17 (2020). <https://doi.org/10.1115/1.4045008>.
- [40] F.B. Spingler, W. Wittmann, J. Sturm, B. Rieger, A. Jossen, Optimum fast charging of lithium-ion pouch cells based on local volume expansion criteria, *J. Power Sources*. 393 (2018) 152–160. <https://doi.org/10.1016/j.jpowsour.2018.04.095>.
- [41] M. Dubarry, G. Baure, A. Devie, Durability and Reliability of EV Batteries under Electric Utility Grid Operations: Path Dependence of Battery Degradation, *J. Electrochem. Soc.* 165 (2018) A773–A783. <https://doi.org/10.1149/2.0421805jes>.
- [42] P.C. Tsai, B. Wen, M. Wolfman, M.J. Choe, M.S. Pan, L. Su, et al., Single-particle measurements of electrochemical kinetics in NMC and NCA cathodes for Li-ion batteries, *Energy Environ. Sci.* 11 (2018) 860–871. <https://doi.org/10.1039/c8ee00001h>.
- [43] X.G. Yang, C.Y. Wang, Understanding the trilemma of fast charging, energy density and cycle life of lithium-ion batteries, *J. Power Sources*. 402 (2018) 489–498. <https://doi.org/10.1016/j.jpowsour.2018.09.069>.
- [44] X. Yang, T. Liu, S. Ge, Y. Leng, D. Wang, X. Yang, et al., Asymmetric Temperature Modulation for Extreme Fast Charging of Lithium-Ion Batteries Asymmetric Temperature Modulation for Extreme Fast Charging of Lithium-Ion Batteries, *Joule*. 3 (2019) 1–18. <https://doi.org/10.1016/j.joule.2019.09.021>.